





# Blocking Palmitoylation of *Toxoplasma gondii* Myosin Light Chain 1 Disrupts Glideosome Composition but Has Little Impact on Parasite Motility

Pramod K. Rompikuntal,<sup>a</sup> Robyn S. Kent,<sup>a</sup> Ian T. Foe,<sup>b</sup> Bin Deng,<sup>d,e</sup>  Matthew Bogyo,<sup>b,c</sup>  Gary E. Ward<sup>a</sup>

<sup>a</sup>Department of Microbiology and Molecular Genetics, University of Vermont Larner College of Medicine, Burlington, Vermont, USA

<sup>b</sup>Department of Pathology, Stanford University School of Medicine, Stanford, California, USA

<sup>c</sup>Department of Microbiology and Immunology, Stanford University School of Medicine, Stanford, California, USA

<sup>d</sup>Department of Biology, University of Vermont, Burlington, Vermont, USA

<sup>e</sup>Vermont Genetics Network Proteomics Facility, University of Vermont, Burlington, Vermont, USA

**ABSTRACT** *Toxoplasma gondii* is a widespread apicomplexan parasite that causes severe disease in immunocompromised individuals and the developing fetus. Like other apicomplexans, *T. gondii* uses an unusual form of substrate-dependent gliding motility to invade cells of its hosts and to disseminate throughout the body during infection. It is well established that a myosin motor consisting of a class XIVa heavy chain (TgMyoA) and two light chains (TgMLC1 and TgELC1/2) plays an important role in parasite motility. The ability of the motor to generate force at the parasite periphery is thought to be reliant upon its anchoring and immobilization within a peripheral membrane-bound compartment, the inner membrane complex (IMC). The motor does not insert into the IMC directly; rather, this interaction is believed to be mediated by the binding of TgMLC1 to the IMC-anchored protein, TgGAP45. Therefore, the binding of TgMLC1 to TgGAP45 is considered a key element in the force transduction machinery of the parasite. TgMLC1 is palmitoylated, and we show here that palmitoylation occurs on two N-terminal cysteine residues, C8 and C11. Mutations that block TgMLC1 palmitoylation completely abrogate the binding of TgMLC1 to TgGAP45. Surprisingly, the loss of TgMLC1 binding to TgGAP45 in these mutant parasites has little effect on their ability to initiate or sustain movement. These results question a key tenet of the current model of apicomplexan motility and suggest that our understanding of gliding motility in this important group of human and animal pathogens is not yet complete.

**IMPORTANCE** Gliding motility plays a central role in the life cycle of *T. gondii* and other apicomplexan parasites. The myosin motor thought to power motility is essential for virulence but distinctly different from the myosins found in humans. Consequently, an understanding of the mechanism(s) underlying parasite motility and the role played by this unusual myosin may reveal points of vulnerability that can be targeted for disease prevention or treatment. We show here that mutations that uncouple the motor from what is thought to be a key structural component of the motility machinery have little impact on parasite motility. This finding runs counter to predictions of the current, widely held “linear motor” model of motility, highlighting the need for further studies to fully understand how apicomplexan parasites generate the forces necessary to move into, out of, and between cells of the hosts they infect.

**KEYWORDS** MyoA, *Toxoplasma*, apicomplexan parasite, motility, myosin, myosin light chain, palmitoylation

**T**oxoplasmosis is among the most widespread and common parasitic infections of humans (1). Acute infection, while typically subclinical and self-limiting, can cause

**Citation** Rompikuntal PK, Kent RS, Foe IT, Deng B, Bogyo M, Ward GE. 2021. Blocking palmitoylation of *Toxoplasma gondii* myosin light chain 1 disrupts glideosome composition but has little impact on parasite motility. mSphere 6:e00823-20. <https://doi.org/10.1128/mSphere.00823-20>.

**Editor** Ira J. Blader, University at Buffalo

**Copyright** © 2021 Rompikuntal et al. This is an open-access article distributed under the terms of the [Creative Commons Attribution 4.0 International license](https://creativecommons.org/licenses/by/4.0/).

Address correspondence to Gary E. Ward, [gary.ward@uvm.edu](mailto:gary.ward@uvm.edu).

**Received** 12 August 2020

**Accepted** 19 April 2021

**Published** 19 May 2021

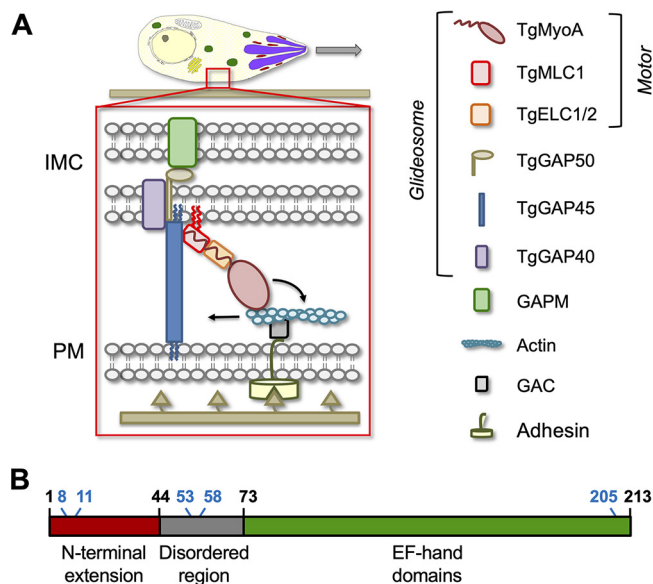


**FIG 1** Schematic illustrations of the glideosome and TgMLC1 domain structure. (A) In the linear motor model of motility (reviewed in reference 9), the TgMyoA motor (TgMyoA and its associated light chains, TgMLC1 and either TgELC1 or TgELC2) is anchored to the parasite's inner membrane complex (IMC) via the acylated protein TgGAP45 and the transmembrane proteins TgGAP40 and TgGAP50. The luminal portion of GAP50 is thought to interact with GAPM, a protein that spans the inner IMC membrane and likely connects the entire glideosome to the underlying parasite cytoskeleton. Short actin filaments located between the parasite plasma membrane and the IMC are connected to ligands on the substrate through a linker protein, possibly GAC, which binds to the cytosolic tails of surface adhesins such as TgMIC2. The TgMyoA motor displaces the actin filaments rearward; because the motor is connected to the IMC and the actin is connected to the substrate, this causes the parasite to move forward relative to the substrate. The depiction of a pair of acyl chains on the N terminus of TgMLC1 (red squiggles) and their interaction with the IMC membrane is based on results reported here. (B) TgMLC1 consists of a 44-amino-acid N-terminal extension, a central disordered region, and four EF hand-like domains, which interact with the tail of TgMyoA. The positions of the five cysteines in the protein are shown in blue; CSS-Palm 4.0 predicted C8 and C11 as likely sites of palmitoylation.

life-threatening disease in immunocompromised individuals and the developing fetus. The causative agent of toxoplasmosis is the protozoan parasite, *Toxoplasma gondii*. *T. gondii* and other parasites of the phylum Apicomplexa, including those that cause malaria and cryptosporidiosis, use an unusual form of substrate-dependent gliding motility to invade into and egress from host cells, migrate across biological barriers, and disseminate through the infected host's tissues (2–4).

Gliding motility in apicomplexan parasites is controlled, at least in part, by an unconventional class XIVa myosin, MyoA (5–8). According to the “linear motor” model of motility that has dominated the field for the last decade (reviewed in reference 9) (Fig. 1A), *T. gondii* MyoA (TgMyoA) and its associated light chains (TgMLC1 and either TgELC1 or TgELC2) are anchored to the parasite's inner membrane complex (IMC) via the acylated glideosome-associated protein, TgGAP45. TgGAP45, in turn, binds to the transmembrane proteins TgGAP40 and TgGAP50. TgGAP50 is firmly immobilized within the IMC lipid bilayer, potentially serving as a fixed anchor against which the motor can generate force (10, 11). This large, heterooligomeric protein complex (TgMyoA, its light chains, TgGAP40, TgGAP45, and TgGAP50) is referred to as the glideosome. In the linear motor model, short actin filaments located between the parasite plasma membrane and the IMC are connected to ligands on the substrate through a glideosome-associated connector protein (GAC) (12) that binds to the cytosolic tails of surface adhesins. Because the motor is anchored into the IMC, when TgMyoA displaces the fixed actin filaments rearward, the parasite moves forward relative to the substrate (Fig. 1A).

TgMLC1 is thought to play two key roles within the *T. gondii* glideosome. First, TgMLC1 binds to the C-terminal tail of TgMyoA to reinforce the motor's lever arm (13–15, 66). The lever arm amplifies small motions at the myosin active site into larger movements that are capable of displacing actin filaments (13, 16). Consistent with this proposed function, recombinant TgMyoA is inactive in *in vitro* motility assays in the absence of TgMLC1 (13 and unpublished data). Second, an interaction between the N-terminal portion of TgMLC1 and the C-terminal portion of TgGAP45 is believed to be the critical link that tethers the motor to the IMC (Fig. 1A) (17–19). Given these proposed functions, it is not surprising that TgMLC1 is an essential protein, and parasites depleted of TgMLC1 are significantly impaired in three-dimensional (3D) motility, invasion, and host cell egress (19, 20).

While the importance of TgMyoA, TgMLC1, and the other glideosome components in motility is well established, recent data have called into question whether they are organized and function as described by the linear motor model and/or whether alternative motility mechanisms exist (19–24). For example, the ability of apicomplexan parasites to rock back and forth on a substrate along their anterior to posterior axis (25–31) is hard to reconcile with the linear motor model, as is the ability of parasites lacking key components of the glideosome to continue moving (19–21; see also reference 32). Given the central importance of motility in the parasite's life cycle and virulence, it is important to fully understand how these proteins work together to generate the forces required to drive parasite movement.

S-palmitoylation is the reversible covalent attachment of a 16-carbon saturated fatty acid via a thioester linkage to cysteine residues of integral and peripheral membrane proteins (33, 34). This widespread posttranslational modification of proteins mediates membrane association and can regulate subcellular localization, trafficking, structure, stability, and diverse aspects of protein function (33, 35–37). Palmitoylation is thought to play an important role in the biology of *T. gondii* and other apicomplexan parasites (38–49). Recent chemical proteomic studies identified several hundred putatively palmitoylated proteins in *T. gondii* (282 unique proteins in one study [49] and 401 in another [39]). Surprisingly, these proteins included all components of the glideosome, including TgMLC1 (39, 49).

TgMLC1 contains five cysteine residues (Fig. 1B), two of which (C8 and C11) are predicted by CSS-Palm 4.0 to be potential sites of palmitoylation. These two cysteines are found within the apicomplexan-specific N-terminal extension of TgMLC1 (Fig. 1B), which is the region of the protein that binds to TgGAP45 (17) (Fig. 1A). Given the important role that TgMLC1 is thought to play in TgMyoA function and motility, we sought to experimentally confirm C8 and/or C11 as the sites of TgMLC1 palmitoylation and to explore the phenotypic consequences of mutations that block this modification.

## RESULTS

**Identification of the sites of palmitoylation on TgMLC1.** To determine whether C8 and/or C11 are sites of palmitoylation on TgMLC1, we replaced the endogenous *TgMLC1* gene with mutant alleles that produce either single (C8S, C11S) or double (C [8,11]S) cysteine-to-serine mutations, rendering these sites nonpalmitoylatable. Each mutant protein was also FLAG tagged at its N terminus (Table 1 provides a complete list of parasite strains used in this study and their designations; see also Fig. S1 in the supplemental material). A fourth parasite line expressing FLAG-tagged wild-type TgMLC1 (WT) was similarly generated. To determine the effect (if any) of the mutations on TgMLC1 palmitoylation, WT, C8S, C11S, and C(8,11)S parasites were grown in medium containing the palmitic acid analog, 17-octadecynoic acid (17-ODYA). FLAG-tagged TgMLC1 was then immunoprecipitated (IP) and subjected to SDS-PAGE. Because 17-ODYA contains a terminal alkyne group, it can be fluorescently tagged with rhodamine-azide through a copper-catalyzed cycloaddition reaction; the amount of rhodamine bound to proteins in the immunoprecipitate subsequently can be

**TABLE 1** Parasite strains used in this study

Strain designation	Relevant genotype
WT	RH $\Delta$ ku80 $\Delta$ mlc1::Flag-MLC1
C8S	RH $\Delta$ ku80 $\Delta$ mlc1::Flag-MLC1 <sup>C8S</sup>
C11S	RH $\Delta$ ku80 $\Delta$ mlc1::Flag-MLC1 <sup>C11S</sup>
C(8,11)S	RH $\Delta$ ku80 $\Delta$ mlc1::Flag-MLC1 <sup>C8S C11S</sup>
C(8,11)A	RH $\Delta$ ku80 $\Delta$ mlc1::Flag-MLC1 <sup>C8A C11A</sup>
WT-MyoATy	RH $\Delta$ ku80 $\Delta$ mlc1::Flag-MLC1 $\Delta$ myoA::MYOA-Ty
C(8,11)S-MyoATy	RH $\Delta$ ku80 $\Delta$ mlc1::Flag-MLC1 <sup>C8S C11S</sup> $\Delta$ myoA::MYOA-Ty

visualized by fluorescence scanning of the gel (49). The amount of rhodamine fluorescence associated with TgMLC1 (31 kDa) was significantly reduced in both the C8S and C11S mutants compared to the WT, with C8S showing a greater reduction than C11S (Fig. 2). In the C(8,11)S double mutant, no 17-ODYA TgMLC1 labeling above background was detectable. In a previous study, C8 and/or C11 were speculated to be sites of palmitoylation on TgMLC1, and parasites expressing a second copy of TgMLC1 in which these two cysteines were mutated to alanines were generated (17). We also generated a C(8,11)A allelic replacement line and found that, like the C(8,11)S double mutation, the C(8,11)A double mutation completely blocked 17-ODYA labeling (Fig. 2). Taken together, these data identify C8 and C11 as essential for, and very likely the sites of, palmitoylation on TgMLC1.

**Subcellular localization of nonpalmitoylatable TgMLC1.** TgMLC1 normally localizes uniformly around the parasite periphery (50). It was previously reported that the C(8,11)A double mutation caused TgMLC1 to mislocalize to the cytosol (17). It was surprising, therefore, that, in our hands, both the C(8,11)S and C(8,11)A mutant proteins remained localized at the parasite periphery (Fig. 3). Reexamination of the images shown in the previous study revealed that most of the C(8,11)A mutant protein (named MLC1<sup>CC-AA</sup>) was indeed also found at the parasite periphery, although there was a

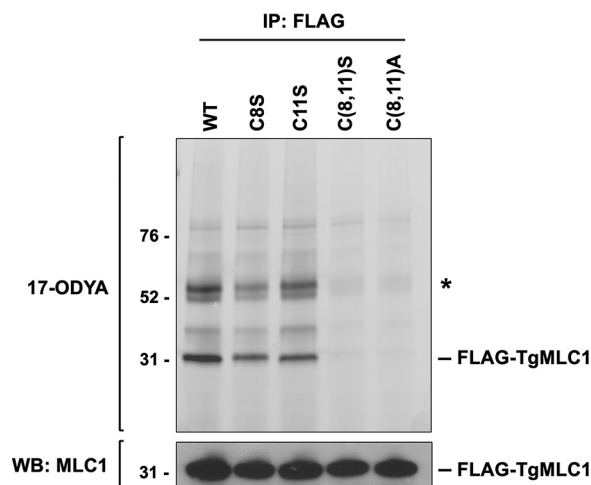


**FIG 2** Cys8 and Cys11 are the likely sites of palmitoylation on TgMLC1. Parasites expressing either wild-type (WT) or mutant FLAG-tagged TgMLC1 were labeled with the palmitic acid analog 17-ODYA, and anti-FLAG affinity resin was then used to pull down FLAG-TgMLC1 and associated proteins. The proteins in the pulldown were resolved by SDS-PAGE and visualized either by rhodamine fluorescence scan (upper) to show the position of 17-ODYA in the gel or by Western blotting (WB) with anti-TgMLC1 (lower). Numbers on the left indicate molecular mass in kDa; only the ~30-kDa portion of the Western blot is shown. The predominant ~31-kDa ODYA-labeled band comigrates with FLAG-TgMLC1; its labeling intensity is reduced in the C8S and C11S single mutants and abolished completely in the C(8,11)S and C(8,11)A double mutants. The Western blot shows similar protein loads in all samples. The asterisk indicates a doublet of ODYA-labeled proteins at ~50 kDa that is pulled down with wild-type FLAG-TgMLC1 but not with either of the double mutants (see the text for details).

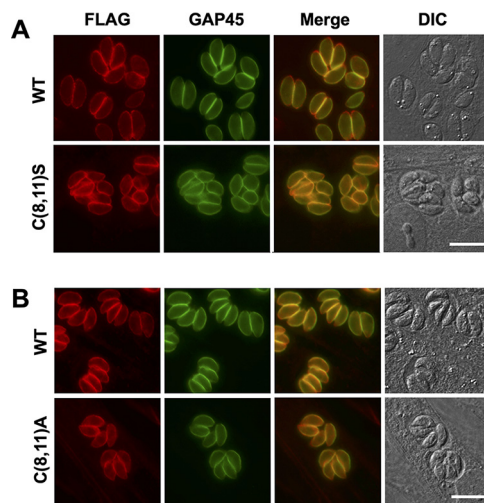


**FIG 3** C(8,11)S and C(8,11)A mutations do not affect localization of TgMLC1 to the parasite periphery. Infected HFF cells were fixed, permeabilized, and stained for FLAG-tagged TgMLC1 (red) or TgGAP45 (green). The corresponding merged and differential interference contrast (DIC) images are also shown. Upper panels compare the localization of WT to C(8,11)S TgMLC1; lower panels compare WT to C(8,11)A TgMLC1. Scale bar, 10  $\mu$ m.

minor amount in the cytosol (for comparison, see the localization of a different mutant in that same study, MLC1<sup>PGF-A1A</sup>, which was clearly cytosolic [17]). The fact that we detect less cytosolic staining with the C(8,11)A allele may reflect differences in protein expression levels in the two studies, since our mutant protein was expressed from the endogenous promoter at the endogenous locus, whereas the previous study expressed the mutant gene in parasites also expressing the wild-type allele (17).

Because the gap between the IMC and the parasite plasma membrane is only  $\sim 25$  nm (17), immunofluorescence localization of TgMLC1 at the parasite periphery cannot distinguish between association with the IMC, the plasma membrane and/or the space between. We therefore treated parasites with *Clostridium septicum*  $\alpha$ -toxin, which causes the parasite plasma membrane to bleb away from the IMC (51), and determined the localization of TgMLC1 relative to TgGAP45 (which remains associated with the IMC [17]) and TgSAG1 (a glycosylphosphatidylinositol [GPI]-linked plasma membrane protein found at the periphery of the blebs [51]). In the absence of  $\alpha$ -toxin, WT TgMLC1 localizes to the parasite periphery along with TgGAP45 and TgSAG1, as expected (Fig. 4A, top row). Following  $\alpha$ -toxin treatment, TgSAG1 is found at the outer edge of the toxin-induced membrane blebs, while both TgGAP45 and TgMLC1 remain associated with the IMC (Fig. 4A, second row). In untreated C(8,11)S mutants, the three proteins again localize to the parasite periphery (Fig. 4A, third row). After  $\alpha$ -toxin treatment, mutant TgMLC1 is associated with the IMC (Fig. 4A, fourth row), but in  $\sim 50\%$  of the parasites it is also found in the space between TgGAP45 and TgSAG1 (Fig. 4A, bottom row, arrow).

Next, we Ty-tagged TgMyoA at the endogenous *TgMyoA* locus in both the WT and C(8,11)S backgrounds using CRISPR/Cas9, creating WT-MyoATy and C(8,11)S-MyoATy (Fig. S2), and did a similar immunofluorescence analysis of Ty-tagged TgMyoA distribution in these parasites after  $\alpha$ -toxin treatment. TgMyoA remained associated with the IMC in WT-MyoATy parasites after  $\alpha$ -toxin treatment, but in the C(8,11)S-MyoATy mutants,  $\sim 50\%$  of the parasites again showed TgMyoA staining both at the IMC and within the bleb (Fig. 4B). Taken together, these results suggest that blocking TgMLC1 palmitoylation decreases the association of TgMLC1 and TgMyoA with the IMC.

**Blocking palmitoylation of TgMLC1 alters its phase partitioning in TX-114.** We also tested whether the mutations that block TgMLC1 palmitoylation alter its phase partitioning in the nonionic detergent Triton X-114 (TX-114). TX-114 efficiently



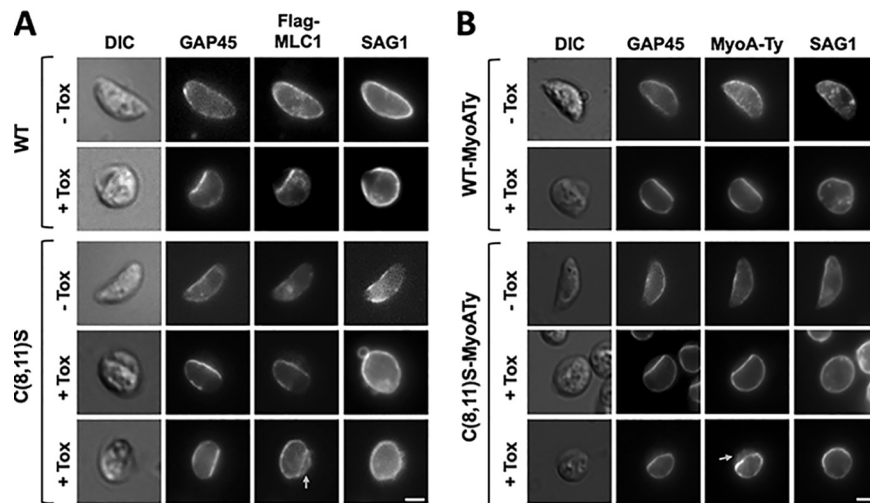


**FIG 4** Blocking TgMLC1 palmitoylation reduces association of TgMLC1 and TgMyoA with the inner membrane complex. (A) WT and C(8,11)S parasites were treated for 3 h with (+Tox) or without (–Tox) *Clostridium septicum*  $\alpha$ -toxin, fixed, and processed for triple immunofluorescence analysis with antibodies against TgGAP45, Flag (to localize TgMLC1-Flag), and TgSAG1. In the absence of  $\alpha$ -toxin, all three proteins were found primarily at the parasite periphery in both WT (top row) and C(8,11)S (third row) parasites. In  $\alpha$ -toxin-treated WT parasites, TgMLC1-Flag remained associated with the IMC (second row). In  $\alpha$ -toxin-treated C(8,11)S parasites, Flag TgMLC1-Flag remained associated with the IMC (fourth row) in 55% of the parasites with a plasma membrane bleb ( $n=84$ ) but was found both at the IMC and in the space between the IMC and the periphery of the plasma membrane bleb (fifth row; arrow) in the remaining 45% of parasites. The corresponding DIC images are also shown. (B) Identical experiment to that in panel A but using WT-MyoATy and C(8,11)S-MyoATy parasites and staining for Ty-tagged TgMyoA rather than TgMLC1-Flag. These populations were nonclonal, so not all parasites stain with anti-Ty. In  $\alpha$ -toxin-treated WT-MyoATy parasites, Flag staining remained associated with the IMC (second row). In  $\alpha$ -toxin-treated C(8,11)S-MyoATy parasites, Flag staining remained associated with the IMC (fourth row) in 59% of the parasites with a plasma membrane bleb ( $n=100$ ) and both at the IMC and in the space between the IMC and the periphery of the plasma membrane bleb (fifth row; arrow) in the remaining 41% of parasites. Scale bars, 2.5  $\mu$ m.

solubilizes most proteins in the parasite at 4°C; when subsequently warmed above the cloud point of the detergent (20°C), intermicellar interactions cause the solution to separate into aqueous and detergent phases, which are enriched in hydrophilic and integral membrane proteins, respectively (52, 53). WT, C8S, and C11S TgMLC1 each partition roughly equally into the aqueous and detergent phases, but the C(8,11)S TgMLC1 double mutant is found almost entirely in the aqueous phase (Fig. 5A and Fig. S3), suggesting a lack of direct membrane association in the absence of palmitoylation. Similar results were seen with the C(8,11)A double mutant (Fig. 5A). As a control, the same samples were probed for TgGRA8, a dense granule protein (54) unrelated to TgMLC1. As expected, the phase partitioning of TgGRA8 was relatively unaffected by the TgMLC1 mutations (Fig. 5B and Fig. S3). These data suggest that the altered localization of palmitoylation-deficient TgMCL1 seen in  $\alpha$ -toxin-treated parasites (Fig. 4) is due at least in part to a decrease in its association with the IMC membrane.

**Effects of TgMLC1 palmitoylation on the composition of the glideosome.** In the 17-ODYA labeling experiments, two prominently labeled ~50-kDa proteins were recovered in the FLAG-WT pulldowns in addition to FLAG-tagged TgMLC1, and these bands were not present in pulldowns from either the C(8,11)S or C(8,11)A double mutant (Fig. 2, asterisk). It was previously suggested that proteins of this size copurifying with WT TgMLC1 but not C(8,11)A are other members of the glideosome complex (17). This hypothesis was strengthened by our subsequent demonstration that most, if not all, glideosome components are, indeed, labeled with 17-ODYA (49). Therefore, we analyzed the FLAG pulldowns of C8S, C11S, and C(8,11)S parasites by Western blotting with antibodies against TgGAP45, TgELC1, and TgMyoA. As expected, TgGAP45 was recovered in the FLAG pulldown from parasites expressing WT TgMLC1; in striking

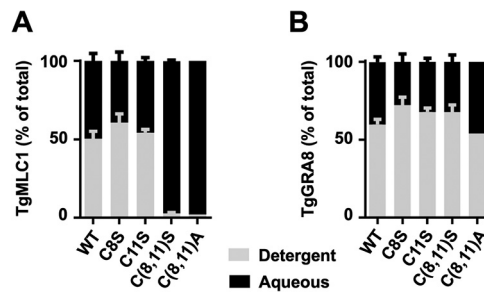


**FIG 5** Blocking TgMLC1 palmitoylation causes the protein to shift into the aqueous phase in Triton X-114. WT, C8S, C11S, C(8,11)S, and C(8,11)A parasites were extracted at 4°C in Triton X-114, and the extracted proteins phase partitioned by shifting the temperature to 20°C. The amounts of TgMLC1 (A) and TgGRA8 (B) recovered in the detergent (gray) and aqueous (black) phases from each sample were determined by quantitative Western blotting (see Fig. S3 for a representative Western blot) and are displayed here as the percentage of the total TgMLC1 recovered in the two phases combined. The data shown are the means and standard errors of the means (SEM) from 2 (C8S, C11S) or 4 (WT, C(8,11)S) independent replicates; C(8,11)A parasites were analyzed once.

contrast, virtually no TgGAP45 was recovered in FLAG pulldowns from parasites expressing C(8,11)S TgMLC1 (Fig. 6A). Pulldown from parasites expressing the C8S single mutation contained intermediate levels of TgGAP45 (Fig. 6A). Quantification of the Western blot signals confirmed these observations and revealed that, concomitant with the decrease in TgGAP45 in the IP of the double mutant, there was a 2- to 3-fold increase in the amount of TgELC1 and TgMyoA recovered (Fig. 6B). Similar results were seen with the C(8,11)A mutant (Fig. S4) (17). The lack of TgGAP45 in the IP from the double mutant is not due to changes in TgGAP45 expression in this parasite line, as Western blots of parasite lysate before immunoprecipitation show similar amounts of TgGAP45 (Fig. 6A and Fig. S4, input). Similarly, anti-TgMyoA Western blots of whole-parasite lysates reveal no changes in the level of expression of TgMyoA in either the C(8,11)S or C(8,11)A mutant parasite lines (Fig. S5). Therefore, blocking TgMLC1 palmitoylation seems to block its ability to interact with TgGAP45 while simultaneously increasing its interaction with TgMyoA and TgELC1.

**Effect of TgMLC1 palmitoylation on parasite motility.** Given the dramatic effect of the C(8,11)S double mutation on the binding of TgMLC1 to TgGAP45, we expected to see a major impact on parasite motility. However, the motility of the double mutant parasites was indistinguishable from parasites expressing WT TgMLC1 in terms of motility initiation, mean displacement, mean speed, and maximum speed (Fig. 7). Track length was slightly shorter in the C(8,11)S parasites but still reached 88% of WT levels. Thus, parasites in which TgMLC1 has lost its ability to interact with TgGAP45 nevertheless show near-normal motility.

This result was unexpected, since, according to the linear motor model of motility, disruption of the interaction between TgMLC1 and TgGAP45 should uncouple TgMyoA from the IMC, rendering it incapable of generating the force required for movement (17) (Fig. 1A). Therefore, we investigated whether the near-normal motility observed in the mutants could be due to changes in the composition of the glideosome that could functionally compensate for the lack of TgMLC1-TgGAP45 interaction, such as the association of TgGAP45 with an alternative light chain/myosin motor or interaction of either TgMLC1 or TgMyoA with alternative GAP proteins.

First, we asked whether TgGAP45 associates with any new proteins in the absence of its normal interaction with TgMLC1. Parasites expressing either WT or C(8,11)S TgMLC1 were metabolically labeled with [<sup>35</sup>S]methionine/cysteine, and the labeled proteins that coimmunoprecipitated with TgGAP45 were resolved by SDS-PAGE, transferred to a polyvinylidene difluoride (PVDF) membrane, and visualized by phosphorimaging. The same membrane used for phosphorimaging was subsequently processed for Western blotting with antibodies against TgMyoA, TgGAP45, and TgMLC1 to determine which of the <sup>35</sup>S-labeled bands comigrate with which of the glideosome proteins.

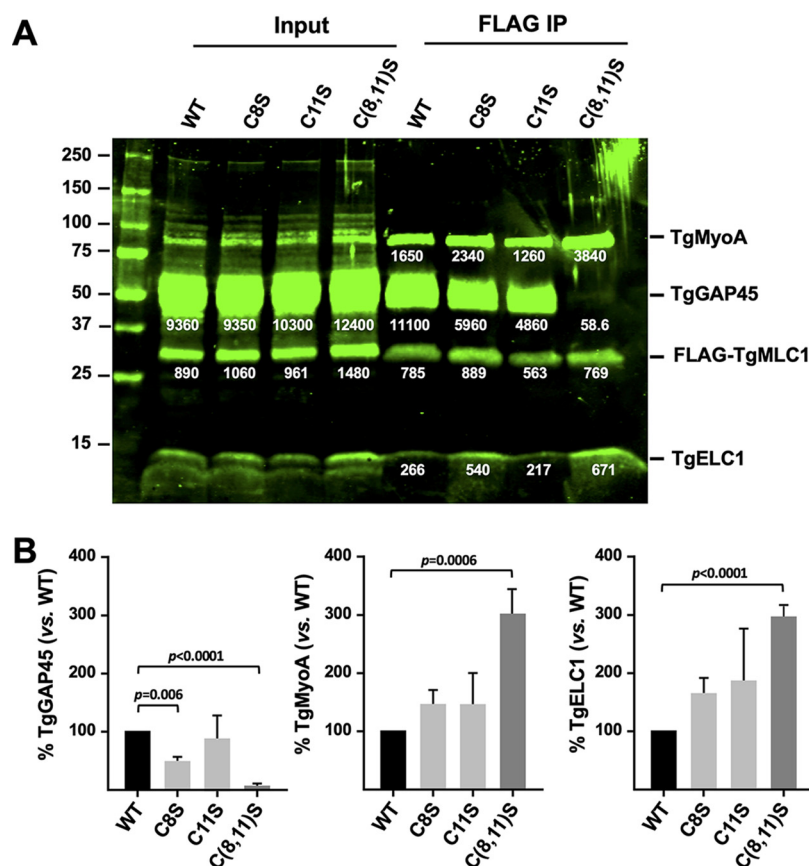


**FIG 6** Blocking TgMLC1 palmitoylation alters the composition of the glideosome. (A) Parasites expressing wild-type or mutant FLAG-tagged TgMLC1 were gently extracted in Triton X-100, and the soluble proteins (Input) were used for anti-FLAG immunoprecipitations (FLAG IP). Immunoprecipitated proteins were resolved by SDS-PAGE and analyzed by sequential Western blotting with anti-TgMyoA, -TgGAP45, -TgMLC1, and -TgELC1; the fluorescent signal intensity of each immunoreactive band is indicated by the white number below the band (relative fluorescence units). Numbers on the left indicate molecular mass in kDa. (B) The signal intensity of TgGAP45, TgMyoA, and TgELC1, immunoprecipitated from each of the mutant parasite lines, is shown relative to the intensity of the corresponding band from the WT line after normalizing to the amount of TgMLC1 recovered in each sample. Shown are the means and SD from either six [WT versus C(8,11)S] or two (WT versus C8S or C11S) independent experiments; differences were assessed using an unpaired two-tailed *t* test.

As expected, both TgMyoA and TgMLC1 coimmunoprecipitate with TgGAP45 from  $^{35}\text{S}$ -labeled WT parasites, whereas neither protein is recovered in TgGAP45 pulldown from C(8,11)S parasites (Fig. 8A), confirming that the motor does not bind to TgGAP45 in the absence of TgMLC1 palmitoylation. No  $^{35}\text{S}$ -labeled bands were detected in the TgGAP45 pulldown from C(8,11)S parasites that were not also present in the pulldown from WT parasites (Fig. 8A). Therefore, TgGAP45 does not appear to interact to any significant/stoichiometric extent with alternate  $^{35}\text{S}$ -labeled myosins or myosin light chains when its interaction with TgMLC1 is disrupted by the C(8,11)S mutation.

We did a similar experiment to see if TgMyoA interacts with an alternative GAP(s) (17) or other proteins in the C(8,11)S mutant, proteins that might serve to anchor TgMyoA into the IMC in the absence of a normal TgMLC1-TgGAP45 interaction. To this end, we analyzed Ty pulldown from  $^{35}\text{S}$ -labeled WT and C(8,11)S parasites expressing Ty-tagged TgMyoA. Ty-tagged TgMyoA and associated TgMLC1 were recovered in the pulldown from both parasite lines, and, as expected, TgGAP45 was only recovered in pulldown from WT parasites (Fig. 8B). Again, no  $^{35}\text{S}$ -labeled proteins were seen to associate with TgMyoA in the C(8,11)S parasites that were not also detected in WT parasites, so there is no evidence that TgMyoA interacts with new binding partners in the C(8,11)S double mutant (Fig. 8B).



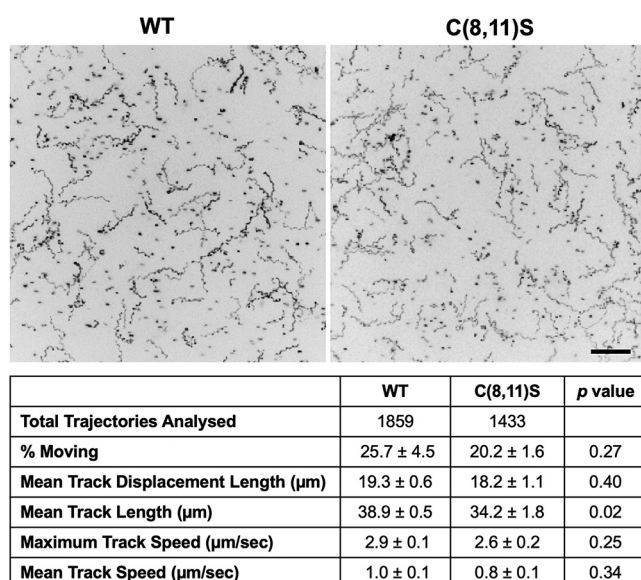


**FIG 7** Mutations that block TgMLC1 palmitoylation and disrupt glideosome composition have little effect on parasite motility. The upper panels show maximum intensity projections of the Hoechst 33342-stained WT or C(8,11)S parasites that moved within a 3-dimensional model extracellular matrix (Matrigel) during 60 s of image capture. Scale bar, 50 μm. The table below shows the motility parameters calculated from three independent motility assays (each consisting of three technical replicates); numbers for each parameter represent the means ± SEM. The total number of trajectories analyzed for each parasite line is also shown. Differences between WT and C(8,11)S parasites for each motility parameter were assessed using an unpaired two-tailed *t* test, and the resulting *P* values are shown in the right column.

Finally, we tested whether the mutant C(8,11)S TgMLC1 itself might interact with a different IMC-anchored protein(s) that could functionally compensate for its lack of interaction with TgGAP45. Anti-FLAG IPs from <sup>35</sup>S-labeled WT and C(8,11)S parasites again confirmed the Western blotting results presented in Fig. 6 and Fig. S4: compared to WT TgMLC1, C(8,11)S TgMLC1 shows both a greatly reduced interaction with TgGAP45 and an increased interaction with TgMyoA (Fig. 8C; quantitative Western blot results from the same sample are shown in Fig. S6). However, in this experiment we also saw a marked increase in the amount of an ~80-kDa <sup>35</sup>S-labeled protein coimmunoprecipitating with C(8,11)S TgMLC1 compared to WT TgMLC1 (Fig. 8C, asterisk). This was intriguing, since TgGAP80, a TgGAP45-related protein that normally interacts with TgMyoC, is also reportedly capable of interacting with TgMLC1 (55). This raised the possibility that an increased interaction between C(8,11)S TgMLC1 and TgGAP80 functionally compensates for the loss of interaction between TgMLC1 and TgGAP45 in the mutant parasites. We therefore repeated the FLAG-TgMLC1 pulldown on a preparative scale and determined the identity of each of the major bands recovered by liquid chromatography-tandem mass spectrometry (LC-MS/MS) (Fig. S7 and Tables S1 and S2). The ~80-kDa band proved to be a truncated form of TgMyoA rather than TgGAP80, and the increased levels of this TgMyoA fragment in the C(8,11)S pulldown paralleled the increased levels of full-length TgMyoA. Taken together, these data argue that the near-normal motility seen in C(8,11)S parasites cannot be explained by the binding of either TgGAP45 or components of the motor to alternative proteins that could functionally compensate for the lack of interaction between TgMLC1 and TgGAP45.

## DISCUSSION

The apicomplexan glideosome plays a critical role in parasite motility, invasion, and virulence (2–4, 56). Recent palmitome analyses have revealed that all known components of the *T. gondii* glideosome are palmitoylated, including TgMyoA, TgMLC1,

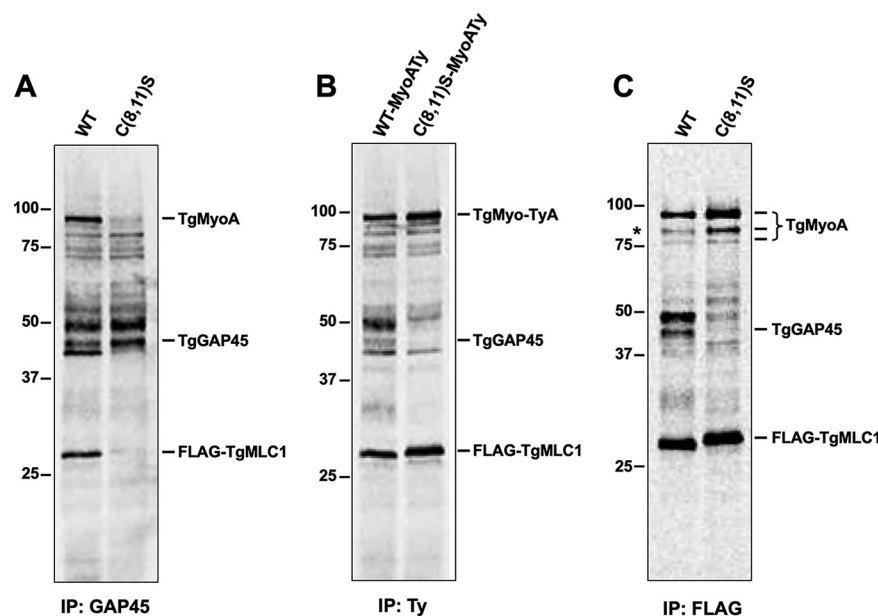


**FIG 8** No changes in glideosome composition that could compensate for the loss of TgGAP45-TgMLC1 interaction are observed in C(8,11)S parasites. Parasites were labeled for 24 h in medium containing [ $^{35}$ S]methionine/cysteine and gently extracted in Triton X-100. Soluble proteins were immunoprecipitated as described below, resolved by SDS-PAGE, transferred to a PVDF membrane, and visualized by phosphorimaging (shown here). The same membrane was subsequently used for Western blotting, probing with antibodies against TgMyoA, TgGAP45, and TgMLC1 (not shown) to determine which  $^{35}$ S-labeled bands corresponded to which glideosome proteins. Numbers on the left of each panel indicate molecular mass in kDa. (A) To test whether TgGAP45 interacts with any new proteins in C(8,11)S parasites,  $^{35}$ S-labeled proteins from WT and C(8,11)S parasites were immunoprecipitated with anti-TgGAP45, resolved by SDS/PAGE, and visualized by phosphorimaging. No bands were detected in the pulldown from C(8,11)S parasites that were not also present in the pulldown from WT parasites. The band migrating immediately below TgGAP45 in the WT sample was recovered in some pulldowns but not others and may represent a breakdown product of TgGAP45 (see Fig. S7). (B) To test whether TgMyoA interacts with any new proteins in the C(8,11)S parasites,  $^{35}$ S-labeled proteins immunoprecipitated using anti-Ty from WT-MyoATy and C(8,11)S-MyoATy parasites were compared. No bands were detected in the pulldown from C(8,11)S parasites that were not also present in the pulldown from WT parasites. (C) To test whether C(8,11)S TgMLC1 interacts with any new proteins compared to WT TgMLC1,  $^{35}$ S-labeled proteins immunoprecipitated using anti-FLAG from WT and C(8,11)S parasites were compared. Asterisk indicates an ~80-kDa band enriched in the FLAG pulldown of C(8,11)S compared to WT; this protein was shown to be a fragment of TgMyoA (see the text). The relative amounts of TgMyoA and TgGAP45 pulled down in panel C were quantified by Western blotting as shown in Fig. S6.

TgELC1, TgGAP40, TgGAP45, and TgGAP50 (39, 49). Widespread glideosome palmitoylation has also been reported in *P. falciparum* (46, 57). Two of the *T. gondii* palmitoyl S-acyl transferases that are essential for parasite survival (TgDHH2 and TgDHH14) localize to the IMC (58, 59) and, therefore, are well situated to play a role in glideosome palmitoylation. The function of palmitoylation of one glideosome component, TgGAP45, was established in an elegant set of experiments by Frenal and colleagues (17). Their study showed that C-terminal palmitoylation of TgGAP45 anchors its C terminus in the IMC, while the other end of the protein is anchored in the plasma membrane via N-terminal palmitoylation and myristoylation. Acylation on the two ends of the protein therefore enables TgGAP45 to bridge the gap between the IMC and the plasma membrane; this determines the spacing between the two membranes and maintains the integrity of the parasite pellicle (17). The function of palmitoylation of other glideosome components is not known, and in most cases the specific residues palmitoylated on these other proteins have not been determined. We have focused here on the function of TgMLC1 palmitoylation.

In the linear motor model of motility, TgMLC1 plays two key roles in force generation: it stabilizes the TgMyoA lever arm (13–15, 66), and it serves as a physical linker

connecting the motor to the IMC by binding to TgGAP45 (17, 18). We show here that TgMLC1 is dually palmitoylated on C8 and C11 (Fig. 2). When we block palmitoylation by mutating these sites to either serine or alanine, TgMLC1 shows decreased association with the IMC (Fig. 4), reduced partitioning into the parasite membrane fraction in Triton X-114 (Fig. 5), and a complete loss of binding to TgGAP45 in coimmunoprecipitation experiments (Fig. 6 and Fig. S4).

How does palmitoylation of C8 and C11 affect the ability of TgMLC1 to bind TgGAP45? The mechanism by which the N terminus of TgMLC1 binds to the C terminus of TgGAP45 (17) is unknown. Direct protein-protein interaction may be involved, as the mutation of two other sets of conserved amino acids near the N terminus of TgMLC1 (D26A/E28A and P36A/G37I/F38A) also interferes with binding to TgGAP45 (17). The presence of the palmitates on C8 and C11 of TgMLC1 might help the interacting N-terminal residues of TgMLC1 transition from a disordered state (14, 15) into a binding-competent configuration. Alternatively, by inserting into the IMC membrane, the acyl chains could position the relevant N-terminal residues of TgMLC1 favorably for interaction with the C terminus of TgGAP45, which is itself attached to the IMC membrane via palmitoylation. It is also possible that the acyl chains on TgMLC1 and TgGAP45 interact directly within the plane of the membrane (15). In any of these cases, blocking TgMLC1 palmitoylation would be expected to inhibit TgMLC1-TgGAP45 interaction, as observed. It is unlikely that palmitoylation is necessary for proper folding and stability of TgMLC1, as appears to be the case with the *P. falciparum* MLC1 homolog, MTIP (46), since (i) we see no evidence for increased degradation of the C(8,11)S mutant compared to WT TgMLC1 (Fig. S5) and (ii) the palmitoylation-deficient mutants continue to bind to TgMyoA (e.g., Fig. 6).

Our data argue against the model that anchoring of the motor in the IMC membrane is mediated solely by the binding of TgMLC1 to TgGAP45, since a fraction of the C(8,11)S mutant TgMLC1, which does not bind to TgGAP45 (Fig. 6), remains associated with the IMC (Fig. 4A). Previous studies with parasites expressing mutant TgGAP45 also argue against the model in which the IMC localization of TgMLC1 is determined by TgGAP45: TgGAP45 lacking its C-terminal palmitoylation sites dissociates from the IMC, yet TgMLC1 remains IMC associated (17). While TgGAP45 may participate in the initial recruitment of TgMLC1 to the space between the plasma membrane and the IMC (10), the subsequent anchoring of the motor in the IMC membrane is likely mediated or reinforced by binding to resident transmembrane proteins of the IMC such as TgGAP40 and TgGAP50 and/or through membrane insertion of the acyl chains present on the different motor components themselves (39, 49).

The most unexpected result of this study was that the motility of parasites expressing C(8,11)S TgMLC1 was, in most aspects, indistinguishable from wild-type parasites (Fig. 7), despite the reduced IMC association and complete disruption of TgMLC1-TgGAP45 interaction caused by this mutation. This observation suggests that the coupling of the motor complex to the IMC via TgGAP45 is unnecessary for force generation by the parasite, directly challenging a fundamental tenet of the linear motor model of motility. The near-normal motility observed in the mutants does not appear to be due to compensatory changes in glideosome composition in response to the mutations [i.e., TgGAP45 does not associate with alternative myosin light chain(s) or myosin motor(s) in the C(8,11)S mutant, and neither the mutant TgMLC1 nor TgMyoA interacts with alternative GAP proteins; Fig. 8]. Another possible explanation for these results is that the nonpalmitoylatable TgMLC1 binds to TgGAP45 in the parasite with a reduced affinity that is sufficient to maintain its association with the IMC and support motility but insufficient to survive extraction in nonionic detergent and immunoprecipitation. However, our phase partitioning and  $\alpha$ -toxin experiments argue strongly against this possibility by independently demonstrating that blocking TgMLC1 palmitoylation does indeed alter TgMLC1 association with the IMC membrane.

In summary, the data presented here demonstrate that TgMLC1 palmitoylation affects its binding to TgGAP45 but plays little to no role in parasite motility, as assayed

by the most sensitive and quantitative assays currently available. The previously reported inhibitory effects of the palmitoylation inhibitor 2-bromopalmitate on parasite motility therefore are not likely due to changes in palmitoylation of TgMLC1, as hypothesized, although changes in the palmitoylation of other glideosome components could be involved (60). While the data presented do not, by themselves, disprove the linear motor model of motility, they add to a growing list of evidence suggesting that the mechanisms underlying apicomplexan parasite motility are more complicated than what is currently encapsulated by the linear motor model (19–24). How the different motility-associated proteins of the parasite interact and work together to generate the forces necessary to drive parasite movement and whether more than one underlying mechanism exists remain important open questions for future study.

## MATERIALS AND METHODS

**Parasite culture.** *T. gondii* tachyzoites were maintained by serial passage in confluent monolayers of human foreskin fibroblasts (HFFs) (ATCC CRL-1634) grown in Dulbecco's modified Eagle's medium (DMEM), supplemented with 10% (vol/vol) heat-inactivated fetal bovine serum (FBS) and 10 mM HEPES, pH 7.0, as previously described (61). The medium was changed to DMEM supplemented with 1% (vol/vol) heat-inactivated FBS and 10 mM HEPES, pH 7.0, prior to infection of confluent HFFs with parasites.

**Generation of TgMLC1 knock-in mutants by allelic replacement.** Mutations were introduced into a previously described *TgMLC1* allelic replacement plasmid (50) using the QuikChange site-directed mutagenesis kit (Agilent Technologies). *Escherichia coli* cells were transformed with the mutagenized plasmids and colonies screened by colony PCR and restriction digestion. The entire open reading frame was sequenced to confirm the presence of only the desired mutation(s). The allelic replacement plasmid was linearized with BglII and PciI and used to transfect RH $\Delta ku80\Delta HXGPRT$  parasites. Successful integration of the mutated gene at the endogenous locus yields phleomycin-resistant, FLAG-positive parasites. Parasites were therefore subjected to two rounds of phleomycin selection, cloned by limiting dilution, and characterized by anti-FLAG immunofluorescence and immunoblotting, as well as diagnostic PCR to confirm correct integration on the chromosome (see Fig. S1 in the supplemental material). Finally, the presence of the desired mutations in individual clones was confirmed by sequencing of genomic DNA.

**Labeling with 17-ODYA.** ODAY labeling was performed as described previously (49).

**Epitope tagging of the TgMyoA locus using CRISPR/Cas9.** To insert the coding sequence for a Ty epitope tag at the C terminus of *TgMyoA*, we constructed plasmid pU6-MyoA, which contains the *TgMyoA* targeting chiRNA under the U6 promoter and *Cas9* under the *TUB1* promoter (62). First, we synthesized a double-stranded DNA oligonucleotide encoding the protospacer sequence used to direct Cas9 to the C-terminal region of *TgMyoA*. To fuse the *TgMyoA* protospacer to the chiRNA of the pU6-universal plasmid, forward and reverse oligonucleotides corresponding to the *TgMyoA* 3' region were annealed by combining them (20  $\mu$ l each, 200  $\mu$ M stocks) in duplex buffer (100 mM potassium acetate, 30 mM HEPES, pH 7.5), heating them to 100°C for 2 min, and then slowly cooling them to 25°C and letting them stand overnight to generate double-stranded product. The duplexed oligonucleotides were dialyzed against deionized water, phosphorylated using T4 polynucleotide kinase, and heat inactivated. Meanwhile, the pU6-universal plasmid (5  $\mu$ g) was linearized by digestion with BsaI, dephosphorylated with Antarctic phosphatase, heat inactivated, and PCR purified. The phosphorylated, duplexed oligonucleotides were then ligated into the pU6-universal plasmid to generate pU6-MyoAPS. Competent *E. coli* DH5- $\alpha$  cells were transformed with the pU6-MyoAPS ligation mixture, and individual colonies with the desired plasmid identified first by colony PCR and then by diagnostic PCR and sequencing. pU6-MyoAPS was transfected along with duplexed, dialyzed homologous recombination (HR) oligonucleotides into WT and C(8,11)S parasites. Ty-positive parasites were identified by immunofluorescence, cloned by limiting dilution, and confirmed as expressing TgMyoA-Ty from the endogenous *TgMyoA* locus by immunofluorescence, diagnostic PCR (see Fig. S2), and sequencing of genomic DNA.

**Immunofluorescence.** HFF cells were infected for 15 h and fixed with 4% (vol/vol) paraformaldehyde in phosphate-buffered saline (PBS) (15 min, 25°C). Fixed cells were washed and permeabilized with PBS containing 0.25% (vol/vol) Triton X-100 for 20 min, washed 3 times with PBS, and blocked (30 min, 25°C) in block buffer (PBS containing 1% [wt/vol] bovine serum albumin). The cells were then incubated for 1 h with primary antibodies diluted as follows with block buffer: mouse monoclonal anti-FLAG (Sigma-Aldrich) at 1:500, rabbit anti-TgGAP45 polyclonal serum (a generous gift from Con Beckers [10]) at 1:1,000, rabbit anti-TgMyoA polyclonal serum (63) at 1:20, and rabbit anti-TgELC1 polyclonal serum at 1:500. Samples were washed 3 times and incubated a further 30 min in goat-anti-rabbit IgG conjugated to Alexa Fluor 546 (Invitrogen) or goat-anti-mouse IgG conjugated to Alexa Fluor 488 (Invitrogen), each diluted 1:500 in block buffer. After four final washes in PBS, fluorescence was visualized by epifluorescence microscopy.

**$\alpha$ -Toxin treatment.** Extracellular tachyzoites were treated for 3 h with trypsin-activated *C. septicum*  $\alpha$ -toxin, as described previously (51). Samples were processed for immunofluorescence as described above, except that blocking and permeabilization were done simultaneously in block buffer containing 0.25% (vol/vol) Triton X-100. Primary antibodies were anti-FLAG diluted 1:200, anti-GAP45 at 1:500, and anti-Ty mouse ascites fluid (a generous gift from Peter Bradley) at 1:500. Secondary antibodies were Alexa Fluor 405-conjugated goat anti-rabbit (for anti-GAP45) at 1:500 and Alexa Fluor 488-conjugated goat anti-mouse (for anti-Ty and anti-Flag) at 1:1,000 (both from Invitrogen). TgSAG1 was detected by

direct immunofluorescence using monoclonal antibody DG52 (a generous gift from David Sibley) directly conjugated to Alexa Fluor 546 (number A20183; ThermoFisher).

**Immunoprecipitation.** For anti-FLAG immunoprecipitations,  $2 \times 10^7$  freshly egressed parasites were extracted for 45 min on ice in 3 ml of FLAG lysis buffer (10 mM imidazole, pH 7.4, 300 mM NaCl, 1 mM EGTA, 5 mM  $MgCl_2$ , 1% [wt/vol] TX-100, 2 mM dithiothreitol, 2 mM ATP) containing 1:100 (vol/vol) protease inhibitors (number P8340; Sigma). The extract was divided into two equal portions, and insoluble material was pelleted at  $10,000 \times g$  (30 min, 4°C). Each  $\sim 1.5$  ml of supernatant was used to resuspend 20  $\mu$ l of packed anti-FLAG M2 affinity resin (Sigma) and then rocked gently overnight at 4°C. After three washes with the FLAG wash buffer (FLAG lysis buffer containing 1:500 [vol/vol] protease inhibitors), bound proteins from the pooled washed resin were eluted with 100  $\mu$ g of FLAG peptide (Sigma) in FLAG wash buffer. Eluates were resolved by SDS-PAGE and proteins visualized by immunoblotting. Primary and secondary (IRDye 680-conjugated anti-rabbit IgG and IRDye 800-conjugated anti-mouse IgG) antibodies were diluted for use in Odyssey blocking buffer (LI-COR). The blots were scanned using an Odyssey CLx infrared imager (LI-COR). Images were processed using Image Studio software (LI-COR). Signal intensities of bands being compared were normalized as described in the figure legends.

**$^{35}S$  metabolic labeling.** For  $^{35}S$  metabolic labeling, confluent HFF cells in a T75 flask were infected with  $1 \times 10^7$  tachyzoites and incubated for 16 to 20 h. The infected cells were then incubated in methionine/cysteine-free DMEM (GIBCO) containing 1% (vol/vol) FBS for 1 h, followed by 24 h in DMEM containing 500  $\mu$ Ci  $^{35}S$ -Easytag mix (Perkin Elmer). Infected cells were detached from the flask using a cell scraper, washed twice with ice-cold PBS, and lysed in FLAG lysis buffer for anti-FLAG immunoprecipitation or TX-100 lysis buffer (1%, vol/vol, TX-100, 50 mM Tris HCl, pH 8.0, 150 mM NaCl, 2 mM EDTA, and 1:200 [vol/vol] protease inhibitors) for anti-Ty and anti-GAP45 immunoprecipitations. Immunoprecipitation was performed as described above except that, after incubation with primary antibody, protein A-Sepharose (Invitrogen) was added and incubated for 1 h with gentle agitation at 4°C to collect the immune complexes. After three washes with either FLAG wash buffer or TX-100 IP wash buffer (1%, vol/vol, TX-100, 50 mM Tris, pH 8.0, 150 mM NaCl, 5 mM EDTA, and 1:500 protease inhibitors), bound proteins were eluted in SDS-PAGE sample buffer by boiling at 100°C for 5 min. Samples were then resolved by SDS-PAGE and transferred to PVDF membranes for phosphorimaging and immunoblotting.

**Phase separation of parasite proteins in Triton X-114.** The phase separation was performed as previously described (52–54). Briefly,  $4 \times 10^8$  tachyzoites were extracted in 1 ml extraction buffer (10 mM Tris-HCl, pH 7.4, 150 mM NaCl, 0.5% [vol/vol] precondensed TX-114 [Pierce] and 1:100 [vol/vol] dilution of protease inhibitors) for 90 min on ice. Insoluble material was removed by centrifugation (twice at  $13,000 \times g$  for 5 min at 4°C). The cleared extract was overlaid onto a 750- $\mu$ l prechilled sucrose cushion (6% [wt/vol] sucrose, 10 mM Tris-HCl, pH 7.4, 150 mM NaCl, and 0.06% [vol/vol] precondensed Triton X-114), incubated for 5 min at 37°C and centrifuged to separate the detergent and aqueous phases (37°C,  $3,000 \times g$ , 5 min). Partitioning was repeated once for each phase, and the collected samples were resolved by SDS-PAGE and analyzed by sequential incubations of a single Western blot with anti-TgMyoA, -TgGAP45, -TgMLC1, and -TgELC1, followed by the appropriate secondary antibodies.

**Motility assays.** 3D motility assays in Matrigel were performed as previously described (50, 64).

**Protein identification by mass spectrometry analysis.** Dried tryptic peptides recovered from excised gel bands (65) were dissolved in 10  $\mu$ l 0.1% formic acid and 2.5% acetonitrile, and 2  $\mu$ l was analyzed on the Thermo Q-Exactive mass spectrometer coupled to an EASY-nLC system (Thermo Fisher). Peptides were separated on a fused silica capillary (12 cm, 100- $\mu$ m inner diameter) packed with a Halo  $C_{18}$  column (2.7- $\mu$ m particle size, 90-nm pore size; Michrom Bioresources) at a flow rate of 300 nl/min. Peptides were introduced into the mass spectrometer via a nanospray ionization source at a spray voltage of 2.2 kV. Mass spectrometry data were acquired in a data-dependent top 10 mode, and the lock mass function was activated ( $m/z$ , 371.1012). Full scans were acquired from  $m/z$  350 to 1,600 at 70,000 resolution (automatic gain control [AGC] target, 1e6; maximum ion time [max IT], 100 ms; profile mode). Resolution for dd-MS<sup>2</sup> spectra was set to 17,500 (AGC target, 1e5) with a maximum ion injection time of 50 ms. The normalized collision energy was 27 eV. A gradient of 0% to 40% acetonitrile (0.1% FA) over 55 min was applied. The spectra were searched against the *T. gondii* protein database (<http://www.toxodb.org/toxo/>) by Proteome Discoverer (PD) 2.0. The search parameters permitted a 10-ppm precursor MS tolerance and a 0.02-Da MS/MS tolerance. Carboxymethylation of cysteines was set up as fixed modification and oxidation of methionine (M) was allowed as a variable modification. Up to three missed tryptic cleavages of peptides were considered with the false discovery rate set to 1% at the peptide level.

## SUPPLEMENTAL MATERIAL

Supplemental material is available online only.

**FIG S1**, TIF file, 1.2 MB.

**FIG S2**, TIF file, 1.5 MB.

**FIG S3**, TIF file, 1.3 MB.

**FIG S4**, TIF file, 0.9 MB.

**FIG S5**, TIF file, 0.2 MB.

**FIG S6**, TIF file, 1.9 MB.

**FIG S7**, TIF file, 0.3 MB.



**TABLE S1**, DOCX file, 0.02 MB.

**TABLE S2**, XLSX file, 0.1 MB.

**TABLE S3**, DOCX file, 0.1 MB.

## ACKNOWLEDGMENTS

We thank Rodney Tweten for his generous gift of  $\alpha$ -toxin and Ying Wai Lam for proteomics advice and support.

This work was supported by U.S. Public Health Service grants AI139201 to G.E.W. and GM111703 to M.B. The Vermont Genetics Network Proteomics Facility is supported through NIH grant P20GM103449 from the INBRE Program of the National Institute of General Medical Sciences.

The funders had no role in study design, data collection and interpretation, or the decision to submit the work for publication.

## REFERENCES

- Montoya JG, Liesenfeld O. 2004. Toxoplasmosis. *Lancet* 363:1965–1976. [https://doi.org/10.1016/S0140-6736\(04\)16412-X](https://doi.org/10.1016/S0140-6736(04)16412-X).
- Barragan A, Sibley LD. 2002. Transepithelial migration of *Toxoplasma gondii* is linked to parasite motility and virulence. *J Exp Med* 195:1625–1633. <https://doi.org/10.1084/jem.20020258>.
- Harker KS, Ueno N, Lodoen MB. 2015. *Toxoplasma gondii* dissemination: a parasite's journey through the infected host. *Parasite Immunol* 37:141–149. <https://doi.org/10.1111/pim.12163>.
- Sibley LD. 2004. Intracellular parasite invasion strategies. *Science* 304:248–253. <https://doi.org/10.1126/science.1094717>.
- Heintzelman MB, Schwartzman JD. 1997. A novel class of unconventional myosins from *Toxoplasma gondii*. *J Mol Biol* 271:139–146. <https://doi.org/10.1006/jmbi.1997.1167>.
- Herm-Götz A, Weiss S, Stratmann R, Fujita-Becker S, Ruff C, Meyhofer E, Soldati T, Manstein DJ, Geeves MA, Soldati D. 2002. *Toxoplasma gondii* myosin A and its light chain: a fast, single-headed, plus-end-directed motor. *EMBO J* 21:2149–2158. <https://doi.org/10.1093/emboj/21.9.2149>.
- Nebi T, Prieto JH, Kapp E, Smith BJ, Williams MJ, Yates JR, III, Cowman AF, Tonkin CJ. 2011. Quantitative in vivo analyses reveal calcium-dependent phosphorylation sites and identifies a novel component of the *Toxoplasma* invasion motor complex. *PLoS Pathog* 7:e1002222. <https://doi.org/10.1371/journal.ppat.1002222>.
- Williams MJ, Alonso H, Enciso M, Egarter S, Sheiner L, Meissner M, Striepen B, Smith BJ, Tonkin CJ. 2015. Two essential light chains regulate the MyoA lever arm to promote *Toxoplasma* gliding motility. *mBio* 6:e00845-15. <https://doi.org/10.1128/mBio.00845-15>.
- Frenal K, Dubremetz JF, Lebrun M, Soldati-Favre D. 2017. Gliding motility powers invasion and egress in apicomplexa. *Nat Rev Microbiol* 15:645–660. <https://doi.org/10.1038/nrmicro.2017.86>.
- Gaskins E, Gilk S, DeVore N, Mann T, Ward G, Beckers C. 2004. Identification of the membrane receptor of a class XIV myosin in *Toxoplasma gondii*. *J Cell Biol* 165:383–393. <https://doi.org/10.1083/jcb.200311137>.
- Johnson TM, Rajfur Z, Jacobson K, Beckers CJ. 2007. Immobilization of the type XIV myosin complex in *Toxoplasma gondii*. *Mol Biol Cell* 18:3039–3046. <https://doi.org/10.1091/mbc.e07-01-0040>.
- Jacot D, Tosetti N, Pires I, Stock J, Graindorge A, Hung YF, Han H, Tewari R, Kursula I, Soldati-Favre D. 2016. An apicomplexan actin-binding protein serves as a connector and lipid sensor to coordinate motility and invasion. *Cell Host Microbe* 20:731–743. <https://doi.org/10.1016/j.chom.2016.10.020>.
- Bookwalter CS, Kelsen A, Leung JM, Ward GE, Trybus KM. 2014. A *Toxoplasma gondii* class XIV myosin, expressed in Sf9 cells with a parasite co-chaperone, requires two light chains for fast motility. *J Biol Chem* 289:30832–30841. <https://doi.org/10.1074/jbc.M114.572453>.
- Powell CJ, Jenkins ML, Parker ML, Ramaswamy R, Kelsen A, Warshaw DM, Ward GE, Burke JE, Boulanger MJ. 2017. Dissecting the molecular assembly of the *Toxoplasma gondii* MyoA motility complex. *J Biol Chem* 292:19469–19477. <https://doi.org/10.1074/jbc.M117.809632>.
- Pazicky S, Dhamotharan K, Kaszuba K, Mertens H, Gilberger T, Svergun D, Kosinski J, Weininger U, Löw C. 2019. Structural role of essential light chains in the apicomplexan glideosome. *bioRxiv* <https://doi.org/10.1101/867499>.
- Warshaw DM. 2004. Lever arms and necks: a common mechanistic theme across the myosin superfamily. *J Muscle Res Cell Motil* 25:467–474. <https://doi.org/10.1007/s10974-004-1767-z>.
- Frenal K, Polonais V, Marq JB, Stratmann R, Limenitakis J, Soldati-Favre D. 2010. Functional dissection of the apicomplexan glideosome molecular architecture. *Cell Host Microbe* 8:343–357. <https://doi.org/10.1016/j.chom.2010.09.002>.
- Bergman LW, Kaiser K, Fujioka H, Coppens I, Daly TM, Fox S, Matuschewski K, Nussenzweig V, Kappe SH. 2003. Myosin A tail domain interacting protein (MTIP) localizes to the inner membrane complex of *Plasmodium* sporozoites. *J Cell Sci* 116:39–49. <https://doi.org/10.1242/jcs.00194>.
- Whitelaw JA, Latorre-Barragan F, Gras S, Pall GS, Leung JM, Heaslip A, Egarter S, Andenmatten N, Nelson SR, Warshaw DM, Ward GE, Meissner M. 18 January 2017. Surface attachment, promoted by the actomyosin system of *Toxoplasma gondii* is important for efficient gliding motility and invasion. *BMC Biol* <https://doi.org/10.1186/s12915-016-0343-5>.
- Egarter S, Andenmatten N, Jackson AJ, Whitelaw JA, Pall G, Black JA, Ferguson DJ, Tardieux I, Mogilner A, Meissner M. 2014. The *Toxoplasma* Acto-MyoA motor complex is important but not essential for gliding motility and host cell invasion. *PLoS One* 9:e91819. <https://doi.org/10.1371/journal.pone.0091819>.
- Andenmatten N, Egarter S, Jackson AJ, Jullien N, Herman JP, Meissner M. 2013. Conditional genome engineering in *Toxoplasma gondii* uncovers alternative invasion mechanisms. *Nat Methods* 10:125–127. <https://doi.org/10.1038/nmeth.2301>.
- Meissner M, Ferguson DJ, Frischknecht F. 2013. Invasion factors of apicomplexan parasites: essential or redundant? *Curr Opin Microbiol* 16:438–444. <https://doi.org/10.1016/j.mib.2013.05.002>.
- Tardieux I, Baum J. 2016. Reassessing the mechanics of parasite motility and host-cell invasion. *J Cell Biol* 214:507–515. <https://doi.org/10.1083/jcb.201605100>.
- Pavlou G, Touquet B, Vigetti L, Renesto P, Bougdour A, Debarre D, Balland M, Tardieux I. 2020. Coupling polar adhesion with traction, spring and torque forces allows high speed helical migration of the protozoan parasite *Toxoplasma*. *ACS Nano* 14:7121–7139. <https://doi.org/10.1021/acsnano.0c01893>.
- Bane KS, Lepper S, Kehrer J, Sattler JM, Singer M, Reinig M, Klug D, Heiss K, Baum J, Mueller AK, Frischknecht F. 2016. The actin filament-binding protein coronin regulates motility in *Plasmodium* sporozoites. *PLoS Pathog* 12:e1005710. <https://doi.org/10.1371/journal.ppat.1005710>.
- Kappe S, Bruderer T, Gant S, Fujioka H, Nussenzweig V, Menard R. 1999. Conservation of a gliding motility and cell invasion machinery in apicomplexan parasites. *J Cell Biol* 147:937–944. <https://doi.org/10.1083/jcb.147.5.937>.
- Munter S, Sabass B, Selhuber-Unkel C, Kudryashev M, Hegge S, Engel U, Spatz JP, Matuschewski K, Schwarz US, Frischknecht F. 2009. *Plasmodium* sporozoite motility is modulated by the turnover of discrete adhesion sites. *Cell Host Microbe* 6:551–562. <https://doi.org/10.1016/j.chom.2009.11.007>.
- Quadt KA, Streichfuss M, Moreau CA, Spatz JP, Frischknecht F. 2016. Coupling of retrograde flow to force production during malaria parasite migration. *ACS Nano* 10:2091–2102. <https://doi.org/10.1021/acsnano.5b06417>.
- Carey KL, Westwood NJ, Mitchison TJ, Ward GE. 2004. A small-molecule approach to studying invasive mechanisms of *Toxoplasma gondii*. *Proc Natl Acad Sci U S A* 101:7433–7438. <https://doi.org/10.1073/pnas.0307769101>.
- Farrell A, Thirugnanam S, Lorentani A, Dvorin JD, Eidell KP, Ferguson DJ, Anderson-White BR, Duraisingh MT, Marth GT, Gubbels MJ. 2012. A DOC2 protein identified by mutational profiling is essential for apicomplexan

- parasite exocytosis. *Science* 335:218–221. <https://doi.org/10.1126/science.1210829>.
31. Hegge S, Münster S, Steinbüchel M, Heiss K, Engel U, Matuschewski K, Frischknecht F. 2010. Multistep adhesion of *Plasmodium* sporozoites. *FASEB J* 24:2222–2234. <https://doi.org/10.1096/fj.09-148700>.
  32. Drewry LL, Sibley LD. 2015. *Toxoplasma* actin is required for efficient host cell invasion. *mBio* 6:e00557. <https://doi.org/10.1128/mBio.00557-15>.
  33. Linder ME, Deschenes RJ. 2007. Palmitoylation: policing protein stability and traffic. *Nat Rev Mol Cell Biol* 8:74–84. <https://doi.org/10.1038/nrm2084>.
  34. Tom CT, Martin BR. 2013. Fat chance! Getting a grip on a slippery modification. *ACS Chem Biol* 8:46–57. <https://doi.org/10.1021/cb300607e>.
  35. Linder ME, Deschenes RJ. 2003. New insights into the mechanisms of protein palmitoylation. *Biochemistry* 42:4311–4320. <https://doi.org/10.1021/bi034159a>.
  36. Salaun C, Greaves J, Chamberlain LH. 2010. The intracellular dynamic of protein palmitoylation. *J Cell Biol* 191:1229–1238. <https://doi.org/10.1083/jcb.201008160>.
  37. Resh MD. 2006. Palmitoylation of ligands, receptors, and intracellular signaling molecules. *Sci STKE* 2006:re14. <https://doi.org/10.1126/stke.3592006re14>.
  38. Beck JR, Fung C, Straub KW, Coppens I, Vashisht AA, Wohlschlegel JA, Bradley PJ. 2013. A *Toxoplasma* palmitoyl acyl transferase and the palmitoylated armadillo repeat protein TgARO govern apical rhoGTP tethering and reveal a critical role for the properties in host cell invasion but not egress. *PLoS Pathog* 9:e1003162. <https://doi.org/10.1371/journal.ppat.1003162>.
  39. Caballero MC, Alonso AM, Deng B, Attias M, de Souza W, Corvi MM. 2016. Identification of new palmitoylated proteins in *Toxoplasma gondii*. *Biochim Biophys Acta* 1864:400–408. <https://doi.org/10.1016/j.bbapap.2016.01.010>.
  40. Child MA, Hall CI, Beck JR, Ofori LO, Albrow VE, Garland M, Bowyer PW, Bradley PJ, Powers JC, Boothroyd JC, Weerapana E, Bogoy M. 2013. Small-molecule inhibition of a depalmitoylase enhances *Toxoplasma* host-cell invasion. *Nat Chem Biol* 9:651–656. <https://doi.org/10.1038/nchembio.1315>.
  41. Corvi MM, Turowski VR. 2019. Palmitoylation in apicomplexan parasites: from established regulatory roles to putative new functions. *Mol Biochem Parasitol* 230:16–23. <https://doi.org/10.1016/j.molbiopara.2019.04.001>.
  42. De Napoli MG, de Miguel N, Lebrun M, Moreno SN, Angel SO, Corvi MM. 2013. N-terminal palmitoylation is required for *Toxoplasma gondii* HSP20 inner membrane complex localization. *Biochim Biophys Acta* 1833:1329–1337. <https://doi.org/10.1016/j.bbamcr.2013.02.022>.
  43. Frenal K, Kemp LE, Soldati-Favre D. 2014. Emerging roles for protein S-palmitoylation in *Toxoplasma* biology. *Int J Parasitol* 44:121–131. <https://doi.org/10.1016/j.ijpara.2013.09.004>.
  44. Fung C, Beck JR, Robertson SD, Gubbels MJ, Bradley PJ. 2012. *Toxoplasma* ISP4 is a central IMC sub-compartment protein whose localization depends on palmitoylation but not myristoylation. *Mol Biochem Parasitol* 184:99–108. <https://doi.org/10.1016/j.molbiopara.2012.05.002>.
  45. Hopp CS, Balaban AE, Bushell ES, Billker O, Rayner JC, Sinnis P. 2016. Palmitoyl transferases have critical roles in the development of mosquito and liver stages of *Plasmodium*. *Cell Microbiol* 18:1625–1641. <https://doi.org/10.1111/cmi.12601>.
  46. Jones ML, Collins MO, Goulding D, Choudhary JS, Rayner JC. 2012. Analysis of protein palmitoylation reveals a pervasive role in *Plasmodium* development and pathogenesis. *Cell Host Microbe* 12:246–258. <https://doi.org/10.1016/j.chom.2012.06.005>.
  47. Tremp AZ, Al-Khattaf FS, Dessens JT. 2017. Palmitoylation of *Plasmodium* alveolins promotes cytoskeletal function. *Mol Biochem Parasitol* 213:16–21. <https://doi.org/10.1016/j.molbiopara.2017.02.003>.
  48. Wetzl J, Herrmann S, Swapna LS, Prusty D, Peter AT, Kono M, Saini S, Nellimarla S, Wong TW, Wilcke L, Ramsay O, Cabrera A, Biller L, Heincke D, Mossman K, Spielmann T, Ungermann C, Parkinson J, Gilberger TW. 2014. The role of palmitoylation for protein recruitment to the inner membrane complex of the malaria parasite. *J Biol Chem* 290:1712–1728. <https://doi.org/10.1074/jbc.M114.598094>.
  49. Foe IT, Child MA, Majmudar JD, Krishnamurthy S, van der Linden WA, Ward GE, Martin BR, Bogoy M. 2015. Global analysis of palmitoylated proteins in *Toxoplasma gondii*. *Cell Host Microbe* 18:501–511. <https://doi.org/10.1016/j.chom.2015.09.006>.
  50. Leung JM, Tran F, Pathak RB, Poupart S, Heaslip AT, Ballif BA, Westwood NJ, Ward GE. 2014. Identification of *T. gondii* myosin light chain-1 as a direct target of TachypleglinA-2, a small-molecule inhibitor of parasite motility and invasion. *PLoS One* 9:e98056. <https://doi.org/10.1371/journal.pone.0098056>.
  51. Wichroski MJ, Melton JA, Donahue CG, Tweten RK, Ward GE. 2002. Clostridium septicum alpha-toxin is active against the parasitic protozoan *Toxoplasma gondii* and targets members of the SAG family of glycosylphosphatidylinositol-anchored surface proteins. *Infect Immun* 70:4353–4361. <https://doi.org/10.1128/iai.70.8.4353-4361.2002>.
  52. Bordier C. 1981. Phase separation of integral membrane proteins in Triton X-114 solution. *J Biol Chem* 256:1604–1607. [https://doi.org/10.1016/S0021-9258\(19\)69848-0](https://doi.org/10.1016/S0021-9258(19)69848-0).
  53. Wichroski MJ, Ward GE. 2003. Biosynthesis of glycosylphosphatidylinositol is essential to the survival of the protozoan parasite *Toxoplasma gondii*. *Eukaryot Cell* 2:1132–1136. <https://doi.org/10.1128/ec.2.5.1132-1136.2003>.
  54. Carey KL, Donahue CG, Ward GE. 2000. Identification and molecular characterization of GRA8, a novel, proline-rich, dense granule protein of *Toxoplasma gondii*. *Mol Biochem Parasitol* 105:25–37. [https://doi.org/10.1016/S0166-6851\(99\)00160-7](https://doi.org/10.1016/S0166-6851(99)00160-7).
  55. Frenal K, Marq JB, Jacot D, Polonais V, Soldati-Favre D. 2014. Plasticity between MyoC- and MyoA-glideosomes: an example of functional compensation in *Toxoplasma gondii* invasion. *PLoS Pathog* 10:e1004504. <https://doi.org/10.1371/journal.ppat.1004504>.
  56. Robert-Paganin J, Robblee JP, Auguin D, Blake TCA, Bookwalter CS, Kremntsova EB, Moussaoui D, Previs MJ, Jousset G, Baum J, Trybus KM, Houdusse A. 2019. *Plasmodium* myosin A drives parasite invasion by an atypical force generating mechanism. *Nat Commun* 10:3286. <https://doi.org/10.1038/s41467-019-11120-0>.
  57. Rees-Channer RR, Martin SR, Green JL, Bowyer PW, Grainger M, Molloy JE, Holder AA. 2006. Dual acylation of the 45 kDa gliding-associated protein (GAP45) in *Plasmodium falciparum* merozoites. *Mol Biochem Parasitol* 149:113–116. <https://doi.org/10.1016/j.molbiopara.2006.04.008>.
  58. Frenal K, Tay CL, Mueller C, Bushell ES, Jia Y, Grainger A, Billker O, Rayner JC, Soldati-Favre D. 2013. Global analysis of apicomplexan protein S-acyl transferases reveals an enzyme essential for invasion. *Traffic* 14:895–911. <https://doi.org/10.1111/tra.12081>.
  59. Dogga SK, Frenal K. 2020. Two palmitoyl acyltransferases involved sequentially in the biogenesis of the inner membrane complex of *Toxoplasma gondii*. *Cell Microbiol* 23:e13212.
  60. Alonso AM, Caceres VM, De Napoli MG, Nieto Guil AF, Angel SO, Corvi MM. 2012. Protein palmitoylation inhibition by 2-bromopalmitate alters gliding, host cell invasion and parasite morphology in *Toxoplasma gondii*. *Mol Biochem Parasitol* 184:39–43. <https://doi.org/10.1016/j.molbiopara.2012.03.006>.
  61. Roos DS. 1996. Molecular genetic tools for the identification and analysis of drug targets in *Toxoplasma gondii*. *Curr Top Microbiol Immunol* 219:247–259. [https://doi.org/10.1007/978-3-642-51014-4\\_22](https://doi.org/10.1007/978-3-642-51014-4_22).
  62. Sidik SM, Hackett CG, Tran F, Westwood NJ, Lourido S. 2014. Efficient genome engineering of *Toxoplasma gondii* using CRISPR/Cas9. *PLoS One* 9:e100450. <https://doi.org/10.1371/journal.pone.0100450>.
  63. Tang Q, Andenmatten N, Hortua Triana MA, Deng B, Meissner M, Moreno SN, Ballif BA, Ward GE. 2014. Calcium-dependent phosphorylation alters Class XIVa myosin function in the protozoan parasite *Toxoplasma gondii*. *Mol Biol Cell* 25:2759–2791. <https://doi.org/10.1091/mbc.E13-11-0648>.
  64. Leung JM, Rould MA, Konradt C, Hunter CA, Ward GE. 2014. Disruption of TgPHIL1 alters specific parameters of *Toxoplasma gondii* motility measured in a quantitative, three-dimensional live motility assay. *PLoS One* 9:e85763. <https://doi.org/10.1371/journal.pone.0085763>.
  65. Krishnamurthy S, Deng B, Del Rio R, Buchholz KR, Treeck M, Urban S, Boothroyd J, Lam YW, Ward GE. 2016. Not a simple tether: binding of *Toxoplasma gondii* AMA1 to RON2 during invasion protects AMA1 from rhomboid-mediated cleavage and leads to dephosphorylation of its cytosolic tail. *mBio* 7:e00754-16. <https://doi.org/10.1128/mBio.00754-16>.
  66. Moussaoui D, Robblee JP, Auguin D, Kremntsova EB, Haase S, Blake TCA, Baum J, Robert-Paganin J, Trybus KM, Houdusse A. 2020. Full-length *Plasmodium falciparum* myosin A and essential light chain PFELC structures provide new anti-malarial targets. *eLife* 9:e60581. <https://doi.org/10.7554/eLife.60581>.